Stabilizing a Low-Dimensional Model of Magnetohydrodynamic Instabilities in Aluminum Electrolysis Cells

Ibrahim Mohammad and Douglas H. Kelley

Abstract

Aluminium (Al) is produced in electrolysis cells that contain two molten, broad, and shallow layers, Al beneath cryolite (bath). A magnetohydrodynamic (MHD) instability known as the metal pad instability (MPI) has been a barrier for reducing anode-to-cathode (ACD) distance and thus decreasing electric losses. The MPI arises from the electromagnetic forces amplifying gravity waves with similar frequencies present at the Al-bath interface. Davidson and Lindsay suggested a mechanical model of the MPI in the form of a compound pendulum with a steady electric current running through it that, in the presence of a vertical magnetic field, couples the pendulum's motion in the two directions. We expand this model to test whether adding an oscillating (AC) current can stabilize the pendulum's motion and consequently have the potential to stabilize Al electrolysis cells. We show that AC current can indeed stabilize the motion, and that stability depends in a complicated way on AC amplitude and frequency.

Introduction

Aluminium electrolysis cells consist of two carbon electrodes with two fluid layers between them: molten cryolite electrolyte (bath) atop molten aluminium metal (Al). The two layers are broad ($\sim 8 \times 3.6$ m, or larger) and shallow ($\sim 5-20$ cm), and the bath is $\sim$4 orders of magnitude more electrically resistive than the Al and $\sim$2 orders of magnitude more than that of the carbon electrodes [1]. During operation, a large, steady current (reduction current or cell amperage) is passed through both layers, reducing aluminium oxide in the bath to Al and producing CO_2 at the anode. However, $\sim$40% of this electrical energy reduces no Al [2] and instead is lost in the form of heat, via Joule heating, concentrated at the highly electrically resistive bath. The losses are directly proportional to the bath height, quantified by the anode-to-cathode distance (ACD), and can be mitigated by reducing the ACD, except doing so below a critical threshold makes the cell unstable [1, 3–8]. To understand why, think of disturbances that naturally exist on the Al-bath interface in the form of long-wavelength gravity waves. Due to the large aspect ratio of the cell and the discrepancy of electrical resistivities of the different materials in it, the waves cause a redistribution of current that is mainly vertical in the bath and horizontal in the Al, flowing from a wave crest towards a wave trough [3, 9]. In the presence of a vertical magnetic field, this redistribution current produces horizontal electromagnetic forces that can excite other gravity waves on the Al-bath interface [1, 5]. This electromagnetic coupling, if strong enough, makes the waves on the Al-bath interface grow in time, creating a magnetohydrodynamic (MHD) instability known as the metal pad instability (MPI) [9, 10] that can cause the electrolysis cells to slosh out of control or the Al to touch the carbon anode shorting the cell. The MPI usually involves the MHD coupling of two or more gravity waves of similar frequencies (resonance) and manifests as a circulating travelling wave [1, 3–6, 9, 11]. The MPI has been extensively studied due to its industrial importance and likelihood to occur in other systems such as liquid metal batteries, a grid-scale energy storage technology [12–14]. Many attempts at suppressing the MPI were made in the past, such as inserting baffles in Al [2, 15] and tilting the anode in synchrony with the Al-bath interface motion [2], with no success. In practice, the MPI is mitigated by careful design of the electrolysis cell [16] and busbar network [17], and by keeping the ACD thick enough.

To provide physical insight to the MPI, a mechanical analogue was given by Davidson and Lindsay [11] in the form of a compound pendulum (see Fig. 1) that captures much of the essential physics: A flat and thin rectangular aluminium

I. Mohammad · D. H. Kelley (✉)
Department of Mechanical Engineering, University of Rochester, Rochester, NY 14627, USA
e-mail: d.h.kelley@rochester.edu

I. Mohammad
e-mail: imohamma@u.rochester.edu

D. Eskin (ed.), *Light Metals 2022*, The Minerals, Metals & Materials Series,
https://doi.org/10.1007/978-3-030-92529-1_68

plate (representing the Al) is attached by a rigid strut to a flat surface (representing the anode) with a poorly conducting electrolyte between them (representing the bath) and a steady current density (representing the reduction current) flowing vertically downwards through the electrolyte to the plate. The plate can swing about both horizontal axes x and y (representing Al-bath interface motion). In the absence of electromagnetic forces, the pendulum's motion in the x and y directions is decoupled and the plate oscillates at its natural gravitational frequency in each direction, ω_x and ω_y, respectively. However, when a vertical magnetic field is imposed and electromagnetic forces are generated, the pendulum's motion in the x and y directions can become coupled: the electromagnetic forces can first shift the gravitational frequencies until they coincide and the plate oscillates at the same frequency in both directions, and then supply energy to the pendulum. In that case, the plate's oscillations grow and become unstable (in analogy to the MPI) [11]. The stability threshold for this model can be derived analytically [11] and offers an accurate ***qualitative*** understanding of the effect of different parameters present in the system on its stability: larger currents, stronger vertical magnetic fields, smaller ACD, and more square cells make the system more unstable. This mechanical analogue is not only powerful in understating the MPI in reduction cells but also has been modified and used to study instabilities in liquid metal batteries [14].

Unstable pendulum motion is a resonance, and resonances can sometimes be frustrated by introducing a new frequency to the system. We hypothesized that adding a time-dependent oscillatory (AC) current component to the pendulum model would suppress its instability. Below, we start by first deriving in detail the equations of motion of the pendulum model when a sinusoidal AC current, with a specified amplitude and frequency, is introduced into the model. Then we solve for the pendulum's motion numerically and show that a previously unstable scenario can be stabilized by the AC current effect.

Mechanical Model

Consider the compound pendulum placed in a Cartesian coordinate system as shown in Fig. 1. It consists of a solid aluminium plate (Al plate) of density ρ_{al} and dimensions L_x, L_y, and H in the x, y, and z directions, respectively, attached to a fixed electrode surface by a strut of height h_0 and negligible mass. The strut pivots, allowing the Al plate to swing about both the x and y axes. The gap, $h(x, y)$, between the Al plate and the electrode surface is filled with a poorly conducting electrolyte, and a vertical magnetic field $\boldsymbol{B}_z$ is imposed as shown. To this point, the model is exactly the same as the one described in [11]. Now, we consider a current density passing vertically downwards through the electrolyte and Al plate, $\boldsymbol{J_0}$, that consists of a steady component and a sinusoidal AC component:

$$\boldsymbol{J_0} = J_0(1 + \beta \sin(\omega_b t))(-\hat{\mathbf{e}}_z) \tag{1}$$

where J_0 is the steady current density amplitude, β is the ratio of the AC current amplitude to that of the steady current, and ω_b is the angular frequency of the AC current. σ_{al}, σ_e are the electrical conductivities of the Al plate and electrolyte, respectively.

Simplifying Assumptions

Following the same consideration as in [11] and in accordance with real aluminium electrolysis cell conditions, we make the following assumptions:

1. The Al plate and electrolyte are broad and shallow such that $(H, h_0) \ll (L_x, L_y)$.
2. The perturbation in the electrolyte thickness, Δh, is very small such that $\Delta h \ll h_0$.
3. The Al plate's periods of oscillations are much greater than the magnetic field diffusion time. This assumption agrees with experimental observations that the characteristic time for the wave motion on the Al-bath interface is much greater than the magnetic field diffusion time in electrolysis cells, implying that the current relaxes to a new equilibrium as the Al-bath interface moves [5].
4. The electrode has a fixed potential Φ_0.
5. The perturbed current, $\boldsymbol{j}$, is purely vertical in the electrolyte. This can be justified by the electrolyte bath hav-

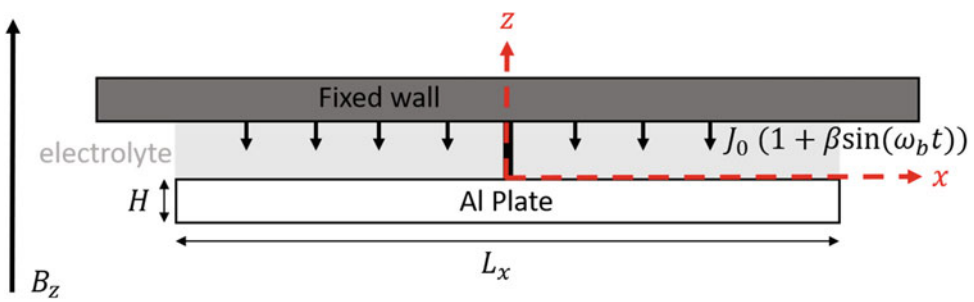

Fig. 1 Schematic diagram of the compound pendulum model. The pendulum can swing about both the x and y axes, with the x-axis as shown and the y-axis pointing into the page

ing a much lower electrical conductivity than Al and electrodes, and the shallow nature of the layer.
6. The Al plate is treated as an equipotential surface with potential $\Phi = 0$ and $\boldsymbol{j}$ is purely horizontal in it. This is due to the Al layer having a much higher electrical conductivity than the bath and electrodes in Al cell and the shallow nature of the layers which make the perturbed current "short" through the Al layer.
7. The perturbed current in the Al plate is much higher than the perturbed current in the electrolyte. Thus, we neglect the perturbed electromagnetic forces in the electrolyte.
8. We ignore the inertia of the electrolyte.
9. The magnetic field induced by $\boldsymbol{j}$ is very small compared to the imposed magnetic field $\boldsymbol{B}_z$ and is neglected.
10. We assume that the vertical magnetic field is constant: $\boldsymbol{B}_z = B_0\hat{\mathbf{e}}_z$.

Equations of Motion

In what follows, we use superscript "e" for quantities related to the electrolyte and "al" for quantities related to the Al plate. We use subscripts to indicate the direction. For example, $\boldsymbol{j}_z^e$ refers to the perturbed current density in the electrolyte along the z-direction. At equilibrium, the Al plate is stationary, the thickness of the electrolyte $h(x, y) = h_0$, and the current density $\boldsymbol{J}_0 = J_0(1 + \beta\sin(\omega_b t))(-\hat{\mathbf{e}}_z)$. Small rotational perturbations of θ_x and θ_y are then applied to the plate about the x and y axes, respectively. Let Δh_x be the perpendicular distance from the top of the plate to the y-axis (see Fig. 2). Then, the angle between the Al plate and the y-axis is θ_x and thus

$$\tan\theta_x = \frac{\Delta h_x}{y}, \tag{2}$$

but, for small θ_x, $\tan\theta_x \approx \theta_x$ so $\Delta h_x \approx y\theta_x$. Similarly, if Δh_y is the perpendicular distance from the top of the plate to the x-axis, $\Delta h_y \approx x\theta_y$. Notice that a rotation of θ_x decreases the electrolyte thickness by Δh_x, while a rotation of θ_y increases the electrolyte thickness by Δh_y. Hence, the perturbed electrolyte thickness is given by

$$h(x, y) = h_0 + \Delta h_y - \Delta h_x \approx h_0 + x\theta_y - y\theta_x. \tag{3}$$

Using assumptions 2, 4, and 6, we find the potential in the electrolyte

$$\Phi(x, y, z) = \frac{\Phi_0 z}{h(x, y)} = \frac{\Phi_0 z}{h_0 + x\theta_y - y\theta_x}. \tag{4}$$

Let $\boldsymbol{J}^e$ denote the total current density in the electrolyte. Then, $\boldsymbol{J}^e = \boldsymbol{J}_0 + \boldsymbol{j}^e$, where $\boldsymbol{j}^e$ is the perturbed current density in the electrolyte. Since $\boldsymbol{J}_0$ and $\boldsymbol{j}^e$ are both purely vertical (assumption 5), then $\boldsymbol{J}^e$ must be as well. Therefore

$$\boldsymbol{J}^e = -\sigma\frac{\partial\Phi}{\partial z}(-\hat{\mathbf{e}}_z) = -\sigma\frac{\Phi_0}{h_0 + x\theta_y - y\theta_x}(-\hat{\mathbf{e}}_z). \tag{5}$$

When $\theta_x = 0 = \theta_y$, the pendulum is at equilibrium and $\boldsymbol{J}^e = \boldsymbol{J}_0 = \frac{-\sigma\Phi_0}{h_0}(-\hat{\mathbf{e}}_z)$. So

$$\boldsymbol{J}^e = \frac{J_0(1 + \beta\sin(\omega_b t))h_0}{h_0 + x\theta_y - y\theta_x}(-\hat{\mathbf{e}}_z). \tag{6}$$

Now we can find the perturbed current density in the electrolyte:

$$\begin{aligned}\boldsymbol{j}^e &= \boldsymbol{J}^e - \boldsymbol{J}_0\\ &= \Big(\frac{-J_0(1 + \beta\sin(\omega_b t))h_0}{h_0 + x\theta_y - y\theta_x} + J_0(1 + \beta\sin(\omega_b t))\Big)(\hat{\mathbf{e}}_z)\\ &= J_0(1 + \beta\sin(\omega_b t))\Big(\frac{x\theta_y - y\theta_x}{h_0 + x\theta_y - y\theta_x}\Big)(\hat{\mathbf{e}}_z).\end{aligned} \tag{7}$$

Let $\epsilon = x\theta_y - y\theta_x$. Then, the Taylor expansion of $\frac{\epsilon}{h_0+\epsilon}$ around $\epsilon = 0$ gives

$$\frac{\epsilon}{h_0 + \epsilon} \approx 0 + \frac{h_0 + \epsilon - \epsilon}{(h_0 + \epsilon)^2}\Big|_{\epsilon=0}(\epsilon - 0) + O(\epsilon^2) \approx \frac{\epsilon}{h_0}.$$

Therefore, the perturbed current density in the electrolyte can be approximated as

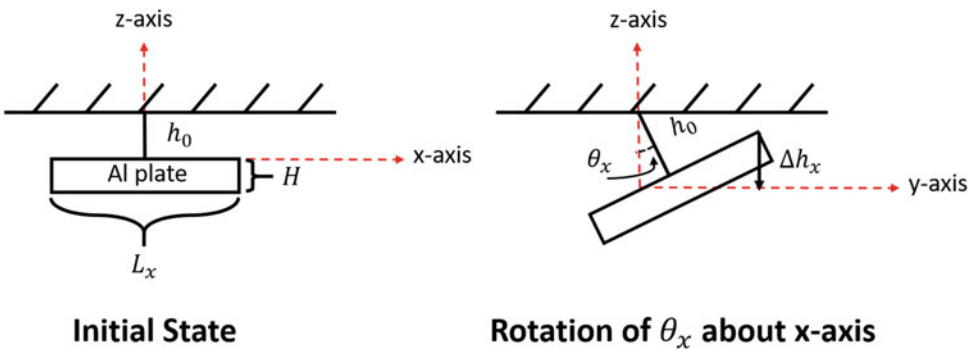

Fig. 2 Pendulum model at initial unperturbed state, and under small rotation about x-axis

$$\boldsymbol{j}^e \approx \frac{J_0(1+\beta\sin(\omega_b t))(x\theta_y - y\theta_x)}{h_0}(\hat{\mathbf{e}}_z) = j^e(\hat{\mathbf{e}}_z). \quad (8)$$

Now, we want to calculate the net flow of perturbed current within the Al plate, and we start by stating the boundary conditions for $\boldsymbol{j}^{al}$, the perturbed current density in the Al plate:

1. $\boldsymbol{j}_z^{al}\Big|_{z=0} = \boldsymbol{j}_z^e$,
2. $\boldsymbol{j}_x^{al}\cdot\hat{\boldsymbol{n}}\Big|_{\text{side boundary}} = 0 = \boldsymbol{j}_y^{al}\cdot\hat{\boldsymbol{n}}\Big|_{\text{side boundary}}$, and
3. $\boldsymbol{j}_z^{al}\Big|_{z=-H} = \mathbf{0}$,

where $\hat{\boldsymbol{n}}$ is an outwards unit normal vector to the Al plate's sides. There are no free charges in the Al plate, so

$$\nabla\cdot\boldsymbol{j}^{al} = \frac{\partial j_x^{al}}{\partial x} + \frac{\partial j_y^{al}}{\partial y} + \frac{\partial j_z^{al}}{\partial z} = 0. \quad (9)$$

We integrate both sides in z and apply boundary conditions 1 and 3 to find

$$\begin{aligned}
&\int_{-H}^{0}\frac{\partial j_x^{al}}{\partial x}\,\mathrm{d}z + \int_{-H}^{0}\frac{\partial j_y^{al}}{\partial y}\,\mathrm{d}z + \int_{-H}^{0}\frac{\partial j_z^{al}}{\partial z}\,\mathrm{d}z = 0\\
&\implies \int_{-H}^{0}\frac{\partial j_x^{al}}{\partial x}\,\mathrm{d}z + \int_{-H}^{0}\frac{\partial j_y^{al}}{\partial y}\,\mathrm{d}z + j_z^{al}\Big|_H^0 = 0\\
&\implies \int_{-H}^{0}\frac{\partial j_x^{al}}{\partial x}\,\mathrm{d}z + \int_{-H}^{0}\frac{\partial j_y^{al}}{\partial y}\,\mathrm{d}z = -j^e.
\end{aligned} \quad (10)$$

Then, integrating Eq. 10 in y, and applying boundary condition 2, we find

$$\begin{aligned}
&\int_{-L_y/2}^{L_y/2}\int_{-H}^{0}\frac{\partial j_x^{al}}{\partial x}\,\mathrm{d}z\,\mathrm{d}y + \int_{-L_y/2}^{L_y/2}\int_{-H}^{0}\frac{\partial j_y^{al}}{\partial y}\,\mathrm{d}z\,\mathrm{d}y = \int_{-L_y/2}^{L_y/2} -j^e\\
&\implies \int_{-L_y/2}^{L_y/2}\int_{-H}^{0}\frac{\partial j_x^{al}}{\partial x}\,\mathrm{d}z\,\mathrm{d}y + \cancelto{0}{\int_{-H}^{0} j_y^{al}\Big|_{-L_y/2}^{L_y/2}\,\mathrm{d}z} = \int_{-L_y/2}^{L_y/2} -j^e\\
&\implies \int_{-L_y/2}^{L_y/2}\int_{-H}^{0}\frac{\partial j_x^{al}}{\partial x}\,\mathrm{d}z\,\mathrm{d}y = -\int_{-L_y/2}^{L_y/2} j^e.
\end{aligned} \quad (11)$$

We integrate Eq. 11 in x from some x' to $\frac{L_x}{2}$. Examining the LHS and applying boundary condition 2, we find

$$\begin{aligned}
&\int_{x'}^{L_x/2}\int_{-L_y/2}^{L_y/2}\int_{-H}^{0}\frac{\partial j_x^{al}}{\partial x}\,\mathrm{d}z\,\mathrm{d}y\,\mathrm{d}x'\\
&\quad= \int_{-L_y/2}^{L_y/2}\int_{-H}^{0}\int_{x'}^{L_x/2}\frac{\partial j_x^{al}}{\partial x}\,\mathrm{d}x'\,\mathrm{d}z\,\mathrm{d}y\\
&\quad\implies \int_{-L_y/2}^{L_y/2}\int_{-H}^{0} -j_x^{al}(x')\,\mathrm{d}z\,\mathrm{d}y \qquad = -I_x^{al}(x'),
\end{aligned}$$

where I_x^{al} represents the net flow of perturbed current in x within the Al plate. Therefore,

$$\begin{aligned}
I_x^{al}(x) &= \int_{x}^{L_x/2}\int_{-L_y/2}^{L_y/2} j^e\,\mathrm{d}y\,\mathrm{d}x\\
&= \frac{J_0(1+\beta\sin(\omega_b t))(\theta_y L_y)}{2h_0}\Big[\Big(\frac{L_x}{2}\Big)^2 - x^2\Big].
\end{aligned}$$

Using the same procedure, the net flow of perturbed current along y inside of the Al plate can be found:

$$I_y^{al}(y) = -\frac{J_0(1+\beta\sin(\omega_b t))(\theta_x L_x)}{2h_0}\Big[\Big(\frac{L_y}{2}\Big)^2 - y^2\Big]. \quad (12)$$

Having found the net perturbed current in the Al plate, we can now find the torques due to the perturbed electromagnetic force. The horizontal perturbed currents within the aluminium plate interact with the unperturbed vertical magnetic field, $\boldsymbol{B_z} = B_0(\hat{\mathbf{e}}_z)$, giving rise to a horizontal perturbed electromagnetic force per unit volume

$$\boldsymbol{f} = \boldsymbol{j}^{al}\times\boldsymbol{B}_z. \quad (13)$$

Its horizontal components are

$$\boldsymbol{f}_x = j_y^{al}\,B_0\,(\hat{\mathbf{e}}_x), \quad (14)$$

$$\boldsymbol{f}_y = -j_x^{al}\,B_0\,(\hat{\mathbf{e}}_y). \quad (15)$$

Hence, the distribution of the electromagnetic force components along the x and y-directions are

$$\begin{aligned}
\boldsymbol{F}_x(y) &= I_y^{al}(y)\,B_0(\hat{\mathbf{e}}_x) = -\frac{J_0 B_0(1+\beta\sin(\omega_b t))(\theta_x L_x)}{2h_0}\\
&\quad\Big[\Big(\frac{L_y}{2}\Big)^2 - y^2\Big](\hat{\mathbf{e}}_x),
\end{aligned} \quad (16)$$

$$\begin{aligned}
\boldsymbol{F}_y(x) &= -I_x^{al}(x)\,B_0(\hat{\mathbf{e}}_y) = -\frac{J_0 B_0(1+\beta\sin(\omega_b t))(\theta_y L_y)}{2h_0}\\
&\quad\Big[\Big(\frac{L_x}{2}\Big)^2 - x^2\Big](\hat{\mathbf{e}}_y).
\end{aligned} \quad (17)$$

Referring to Fig. 3, the distributions of the torques arising from the electromagnetic forces about the pivot, along the x and y directions, respectively, are

$$\boldsymbol{\tau}_x(x) = r_\perp^x F_y(x)(-\hat{\mathbf{e}}_z\times\hat{\mathbf{e}}_y) = (h_0 + \frac{H}{2})F_y(x)\,(\hat{\mathbf{e}}_x), \quad (18)$$

$$\boldsymbol{\tau}_y(y) = r_\perp^y F_x(y)(-\hat{\mathbf{e}}_z\times\hat{\mathbf{e}}_x) = -(h_0 + \frac{H}{2})F_x(y)\,(\hat{\mathbf{e}}_y). \quad (19)$$

The net torques are obtained by integrating Eq. 18 along the x direction and Eq. 19 along the y direction:

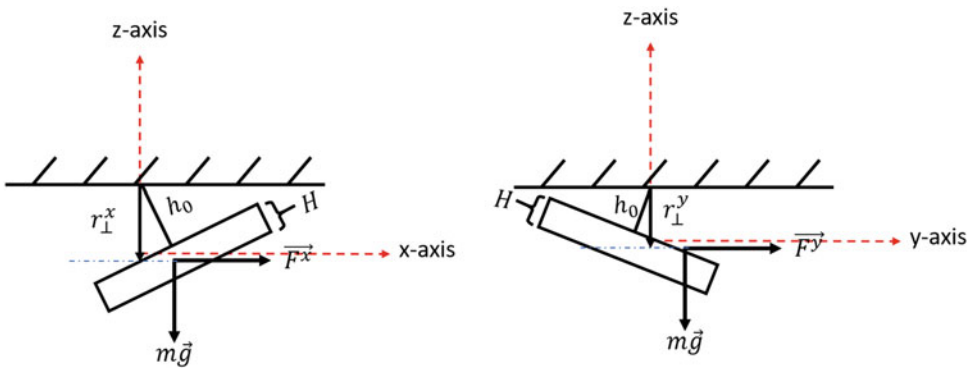

Fig. 3 Only the electromagnetic and gravitational forces have a net non-zero torque with respect to the pivot

$$\tau_x^{\text{net}} = \int_{-L_x/2}^{L_x/2} \tau_x(x)\,\mathrm{d}x = -(h_0 + \frac{H}{2})\frac{J_0 B_0(1+\beta\sin(\omega_b t))(\theta_y L_y)}{h_0}\frac{(L_x)^3}{12}(\hat{\mathbf{e}}_x), \tag{20}$$

$$\tau_y^{\text{net}} = \int_{-L_y/2}^{L_y/2} \tau_y(y)\,\mathrm{d}y = (h_0 + \frac{H}{2})\frac{J_0 B_0(1+\beta\sin(\omega_b t))(\theta_x L_x)}{h_0}\frac{(L_y)^3}{12}(\hat{\mathbf{e}}_y). \tag{21}$$

With the net torques due to the perturbed electromagnetic force found, we can derive the Al plate's equations of motion by considering the conservation of angular momentum about the horizontal axes parallel to x and y axes when the Al plate is at $\theta_x = 0 = \theta_y$, and passing through the pivot. As shown in Fig. 3, the only torques acting on the plate are the ones due to the electromagnetic and gravity forces, so using Newton's second law for rotation

$$I_{xx}\boldsymbol{\alpha}_x = \sum \boldsymbol{\tau} = \boldsymbol{\tau}_x^{\text{net}} + \boldsymbol{\tau}_x^{\text{gravity}}, \tag{22}$$

$$I_{yy}\boldsymbol{\alpha}_y = \sum \boldsymbol{\tau} = \boldsymbol{\tau}_y^{\text{net}} + \boldsymbol{\tau}_y^{\text{gravity}}, \tag{23}$$

where $\boldsymbol{\alpha_x} = \ddot{\theta}_x\hat{\mathbf{e}}_x$ and $\boldsymbol{\alpha_y} = \ddot{\theta}_y\hat{\mathbf{e}}_y$ are the angular accelerations with $\ddot{()}$ indicating the second derivative in time, I_{xx} and I_{yy} are the moments of inertia of the rectangular Al plate

$$I_{xx} = \rho_a L_x L_y H\Big[\frac{L_y^2}{12} + \cancel{\frac{H^2}{12}}^{small} + \cancel{(h_0 + \frac{H}{2})^2}^{small}\Big], \tag{24}$$

$$I_{yy} = \rho_a L_x L_y H\Big[\frac{L_x^2}{12} + \cancel{\frac{H^2}{12}}^{small} + \cancel{(h_0 + \frac{H}{2})^2}^{small}\Big], \tag{25}$$

and $\boldsymbol{\tau}_x^{\text{gravity}}$, $\boldsymbol{\tau}_y^{\text{gravity}}$ are the torques due to gravity

$$\boldsymbol{\tau}_x^{\text{gravity}} = \boldsymbol{r}_\perp \times m\boldsymbol{g} = \rho_{al} L_x L_y H g(h_0 + \frac{H}{2})\theta_x\,(-\hat{\mathbf{e}}_x) \tag{26}$$

$$\boldsymbol{\tau}_y^{\text{gravity}} = \boldsymbol{r}_\perp \times m\boldsymbol{g} = \rho_{al} L_x L_y H g(h_0 + \frac{H}{2})\theta_y\,(-\hat{\mathbf{e}}_y). \tag{27}$$

Substituting Eqs. 20, 21, 24, 25, 26, and 27 into 22 and 23 and rearranging yields

$$\ddot{\gamma}_x + \omega_x^2\gamma_x = -a(1+\beta\sin(\omega_b t))\gamma_y, \tag{28}$$

$$\ddot{\gamma}_y + \omega_y^2\gamma_y = a(1+\beta\sin(\omega_b t))\gamma_x, \tag{29}$$

where $\gamma_x = \frac{\theta_x}{L_x^2}$ and $\gamma_y = \frac{\theta_y}{L_y^2}$ are normalized angles, $\omega_x^2 = \frac{g(h_0+\frac{H}{2})}{L_y^2/12}$ and $\omega_y^2 = \frac{g(h_0+\frac{H}{2})}{L_x^2/12}$ are the squares of the natural frequencies of the pure gravitational oscillations in the x and y directions respectively, and $a = \frac{(h_0+H/2)J_0B_0}{\rho_{al}Hh_0}$ is the coupling parameter.

Numerical Solution

We solved the coupled system of ordinary differential equations, Eqs. 28, 29, describing the Al plate's motion numerically using MATLAB. We used the initial conditions of small rotations θ_x, θ_y, and zero angular velocities $\dot{\theta}_x = 0 = \dot{\theta}_y$. We set the Al plate dimensions to $H = 0.2$ m, $h_0 = 0.045$ m, $L_x = 11$ m, and $L_y = 2.7$ m and used $g = 9.81$ m/s^2. We chose these values to reasonably mimic the lateral dimensions and fluid layer thicknesses in an Al electrolysis cell. We calculated the natural gravitational frequencies of the Al plate to be $\omega_x = 1.5302$ rd/s and $\omega_y = 0.3756$ rd/s.

We first solved for the simple case for $a = 0$ which decouples the Al plate's motion about the x and y directions. This can be thought of as having no current at all ($J_0 = 0$) or no magnetic field ($B_0 = 0$) which implies that there's no electromagnetic forces present. Gravitational forces are the only ones present, and we expect the Al plate would oscillate with frequency ω_x in x and ω_y in y. Our numerical results for $a = 0$ also show that this is the case (Fig. 4). γ_x and γ_y are pure sinusoidal oscillations (Fig. 4a, b). The power spectrum of each shows that the oscillation frequencies coincide with ω_x and ω_y (Fig. 4c).

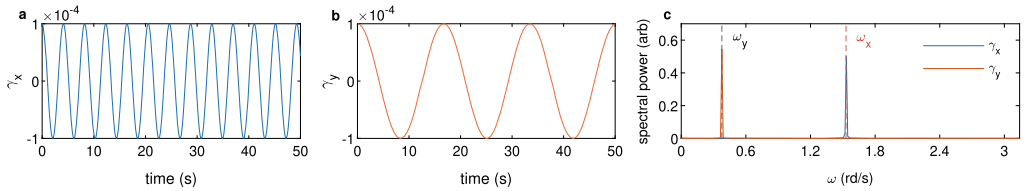

Fig. 4 Numerical solutions for the decoupled case $a = 0$. **a**, γ_x oscillates in time at a single frequency. **b**, γ_y oscillates in time at a single frequency that is lower than that of γ_x. **c** The power spectrum of both γ_x and γ_y shows that each oscillates exactly at its pure gravitational frequency

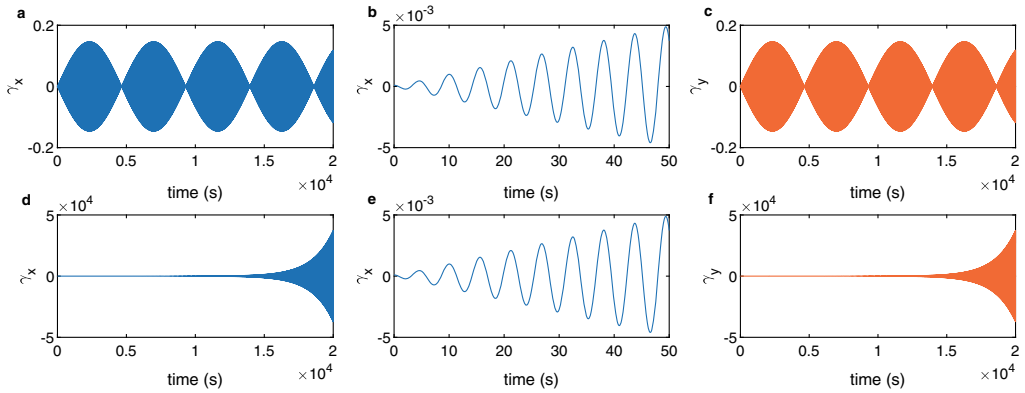

Fig. 5 Numerical solutions at a slightly above and below a_{crit}. **a**, $a = 1.100205$, the Al plate is stable with γ_x oscillating in time and beating phenomenon is present. The regions appearing in solid blue indicate oscillations too fast to be individually visible. **b**, an enlargement of the same data as (a) plotted for only 50 s. The oscillations inside the amplitude envelope can now be seen. **c**, γ_y is also stable, behaving the same as γ_x. **d**, $a = 1.100207$, the Al plate is unstable with the amplitude of γ_x increasing exponentially in time. The regions appearing in solid blue indicate oscillations too fast to be individually visible. **e**, an enlargement of the same data as (d) plotted for only 50 s. **f**, γ_y is also unstable, behaving the same as γ_x

Next, we solved for the steady current case by setting $\beta = 0$ which eliminates the oscillatory component of the current. This case is originally studied in [11], where it was shown that the onset of instability occurs when the coupling parameter "a" exceeds the critical value

$$a_{\text{crit}} = \frac{|\omega_x^2 - \omega_y^2|}{2}. \tag{30}$$

For our values of ω_x and ω_y, the critical coupling parameter $a_{\text{crit}} = 1.100206$. Our numerical results for $a = 1.100205$ and $a = 1.100207$, slightly below and above a_{crit}, also show a transition in stability. At $a = 1.100205$, γ_x oscillates stably and the amplitude is enveloped by a slowly varying oscillation (Fig. 5a); the beating phenomenon is present. Plotting only the first 50 s (Fig. 5b) shows the oscillations happening at a higher frequency inside the amplitude envelope. γ_y behaves the same as γ_x (Fig. 5c). At $a = 1.100207$, γ_x is unstable with the amplitude growing exponentially in time (Fig. 5d). γ_x reaches ~25000, which would exceed $\theta_x = \pi/2$ and definitely violate the small-angle approximation. So, the normalized angles shouldn't be taken literally but the exponential growth in amplitude is really an indicator of instability. Plotting only the first 50 s (Fig. 5e) shows the oscillations of γ_x. γ_y is also unstable (Fig. 5f).

We solved again for $a = 1.100207$ but with an AC current present ($\beta \neq 0$). We checked the stability of γ_x and γ_y

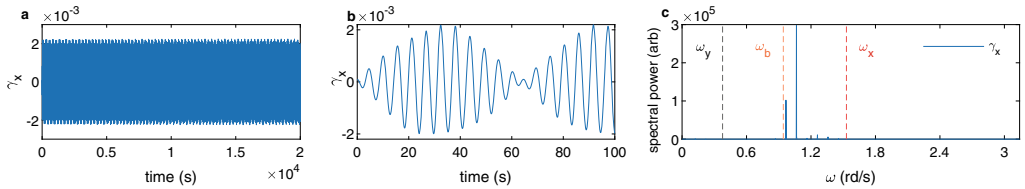

Fig. 6 Numerical solutions at $a = 1.100207$ with an AC current of $\beta = 0.1$ and $\omega_b = 0.94$ rd/s. **a**, γ_x oscillating in time stably. The regions appearing in solid blue indicate oscillations too fast to be individually visible. **b**, an enlargement of the same data as (a) plotted for only 100 s. The oscillations inside the amplitude envelope can now be seen. **c**, The power spectrum of γ_x shows two frequencies, one near the AC frequency

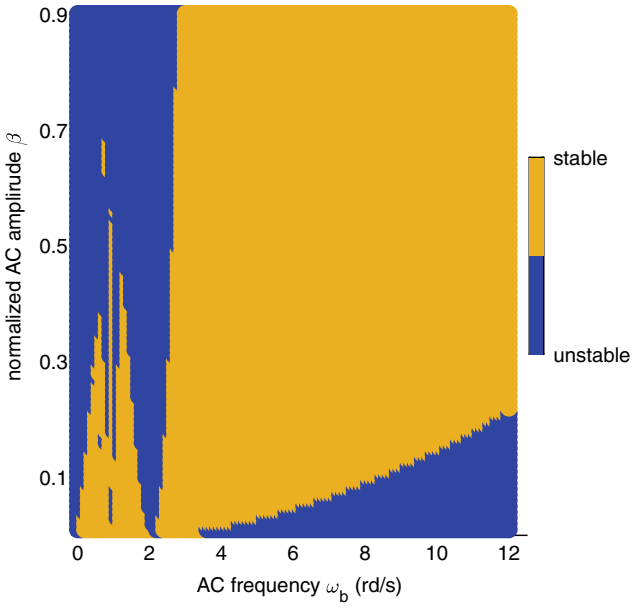

Fig. 7 (β, ω_b) phase space. The model is stable for many pairs of AC frequency and amplitude. The stable pairs cluster at two distinct regions

for a range of AC currents, each with a different amplitude and frequency. We found that using an AC current frequency $\omega_b = 0.94$ rd/s and $\beta = 0.1$ (10% of the steady current) stabilized the motion, where γ_x (Fig. 6a–b) and γ_y no longer grow in time. The power spectrum of γ_x shows two dominant frequencies present: one near the AC frequency of 0.94 rd/s, and the other near the root-mean-square of the natural gravitational frequencies of ∼1.1 rd/s (Fig. 6c). We summarize the stability at $a = 1.100207$ for different pairs of AC amplitude and frequency, (β, ω_b), in Fig. 7, where we varied β from 0.01 to 0.9 in steps of 0.01 and ω_b from 0 rd/s to 12 rd/s in steps of 0.1 rd/s. At $\omega_b = 0$ rd/s, the current is only steady and the Al plate motion is expected to be unstable for all β, as shown. For $\omega_b \neq 0$, two distinct regions of stability emerge. One near lower frequencies that almost looks like a triangle whose base is centered at ∼1 rd/s. Having a lower amplitude seems to be better for stability. The other region is much bigger and at higher frequencies and seems to be bounded by two curves, one of which is almost a vertical line at $\omega_b \sim 2.5$ rd/s. At higher frequencies, a higher amplitude seems to better. Overall, the (β, ω_b) phase space portrait looks a bit like Arnold tongue [18].

Discussion

We derived the equations of motion of the mechanical analogue [11] of the MPI but with an added sinusoidal AC current component added to the steady one. We showed that adding the AC current successfully stabilized the model at various AC frequencies ω_b and amplitudes β. The driving AC frequency was present in the stabilized oscillations power spectrum, in addition to the root-mean-square (RMS) frequency of the natural gravitational frequencies ω_x and ω_y. The presence of the RMS frequency can also be seen by taking the sum and difference of Eqs. 28 and 29, and then rewriting in terms of the new variables $\Gamma_1 = \gamma_x + \gamma_y$ and $\Gamma_2 = \gamma_x - \gamma_y$.

We also found that the stability depends in a complicated way on ω_b where distinct regions of stability occur. For every frequency we checked but one, there was some β that stabilized the cell, with lower β being generally better for stabilizing at lower frequencies and vice versa. The one frequency that didn't stabilize the system was ∼1.9 rd/s, close to the sum of the natural gravitational frequencies ω_x and ω_y. We suspect that when driving at this frequency, a frequency matching parametric instability occurs.

Our choice of model dimensions, H , h_0, L_x, and L_y, was to mimic similar dimensions in an Al electrolysis cells. Changing any of the dimensions would change the natural gravitational frequencies and consequently the critical coupling parameter a_{crit}. When we solved for the Al plate's motion, we would set the value of the coupling parameter a rather than calculating it for values of J_0 and B_0 that would be similar to those in Al cells. Doing so would have given a values so low that the Al plate is always stable. Thus, the results from this mechanical model should be only considered in a qualitative rather than a quantitative manner when translating results to real Al cells. For example, having a larger aspect ratio of L_x/L_y would increase the difference between the natural gravitational frequencies and consequently indicate a more stable scenario. This translates well to Al cells where a large aspect ratio is desired for stability [1].

Also, the mechanical model reduces the real two-fluid layer system in Al electrolysis cells from one with an infinite number of degrees of freedom to one with only two. In Al cells, there are many gravitational frequencies and many couplings between them can occur to trigger the MPI [1, 5, 9, 9]. The mechanical model also fails to account for damping effects in Al cells, such as viscosity and the friction between the fluid layer and the electrode, which would most certainly impact stability. The mechanical model is only a low-dimensional representation of the physical phenomena happening.

The system of Eqs. 28, 29 is canonically a periodic linear differential equation system of the form $\dot{\boldsymbol{y}} = A(t)\boldsymbol{y}$, where the matrix $A(t)$ is periodic with period $\frac{2\pi}{\omega_b}$. Analytical techniques such as Floquet theory [19] can be used to study the stability of the system and perhaps outline the distinct stable regions present in the (β, ω_b) phase space for a given coupling parameter a in future work. Beyond the mechanical model, testing whether AC currents can stabilize actual Al electrolysis cells is very interesting. A good

start is to perform high fidelity numerical simulations of Al cells, such as those done with MHD-Valdis [20, 21]. We did so in [22] and verified that AC currents can suppress the MPI in simulation.

References

1. Bojarevics and M. V. Romerio, "Long waves instability of liquid-metal electrolyte interface in aluminum electrolysis cells - a generalization of sele criterion," *European journal of mechanics, B, Fluids*, vol. 13, no. 1, pp. 33–56, 1994.
2. P. Davidson, "Overcoming instabilities in aluminium reduction cells: a route to cheaper aluminium," *Materials Science and Technology*, 2000.
3. T. Sele, "Instabilities of the metal surface in electrolytic alumina reduction cells," *Metallurgical Transactions B*, vol. 8, no. 4, pp. 613–618, 1977.
4. A. D. Sneyd and A. Wang, "Interfacial instability due to mhd mode coupling in aluminium reduction cells," *Journal of fluid mechanics*, vol. 263, pp. 343–360, 1994.
5. P. Davidson, "An energy analysis of unstable, aluminium reduction cells," *European Journal of Mechanics B-fluids*, vol. 13, pp. 15–32, 1994.
6. N. Urata, "Wave mode coupling and instability in the internal wave in aluminum reduction cells," in *TMS Annual Meeting*, pp. 455–460, 2005.
7. A. Lukyanov, G. El, and S. Molokov, "Instability of mhd-modified interfacial gravity waves revisited," *Physics letters. A*, vol. 290, no. 3, pp. 165–172, 2001.
8. O. Zikanov, A. Thess, P. Davidson, and D. Ziegler, "A new approach to numerical simulation of melt flows and interface instability in hall-héroult cells," *Metallurgical and Materials Transactions B*, vol. 31, pp. 1541–1550, 2000.
9. N. Urata, "Magnetics and metal pad instability," in *Light Metals: Proceedings of Sessions, AIME Annual Meeting*, pp. 581–591, 1985.
10. V. Bojarevics and J. W. Evans, *Mathematical Modelling of Hall-Héroult Pot Instability and Verification by Measurements of Anode Current Distribution*, pp. 783–788. Hoboken, NJ, USA: John Wiley & Sons, Inc, 2015.
11. P. A. DAVIDSON and R. I. LINDSAY, "Stability of interfacial waves in aluminium reduction cells," *Journal of Fluid Mechanics*, vol. 362, pp. 273–295, 1998.
12. G. M. Horstmann, N. Weber, and T. Weier, "Coupling and stability of interfacial waves in liquid metal batteries," *Journal of Fluid Mechanics*, vol. 845, pp. 1–35, 2018.
13. N. Weber, P. Beckstein, W. Herreman, G. M. Horstmann, C. Nore, F. Stefani, and T. Weier, "Sloshing instability and electrolyte layer rupture in liquid metal batteries," *Physics of fluids (1994)*, vol. 29, no. 5, pp. 54101–16, 2017.
14. O. Zikanov, "Metal pad instabilities in liquid metal batteries," *PHYSICAL REVIEW E*, vol. 92, no. 6, 2015.
15. A. Pedcenko, S. Molokov, and B. Bardet, "The effect of "wave breakers" on the magnetohydrodynamic instability in aluminum reduction cells," *Metallurgical and Materials Transactions B*, vol. 48, no. 1, pp. 6–10, 2017.
16. G. Politis and J. Priede, "Fractality of metal pad instability threshold in rectangular cells," *Journal of fluid mechanics*, vol. 915, 2021.
17. M. Dupuis, J. Chaffy, and B. Langon, "A new aluminium electrolysis cell busbar network concept," 2015.
18. F. Schilder, and B. Peckham, "Computing Arnol'd tongue scenarios," *Journal of Computational Physics*, vol. 220, no. 2, pp. 932–951, 2007.
19. J. Nathan Kutz, "*Advanced Differential Equations: Asymptotics & Perturbations*," http://arxiv.org/licenses/nonexclusive-distrib/1.0, 2020.
20. V. Bojarevics and K. Pericleous, "Time dependent electric, magnetic and hydrodynamic interaction in aluminium electrolysis cells," in *Fifth International Conference on CFD in the Process Industries CSIRO*, 2006.
21. M. Dupuis and V. Bojarevics, "Analyzing the impact on the cell stability power modulation on a scale of minutes," in *ALUMINIUM SMELTING INDUSTRY*, pp. 54–57, 2021.
22. I. Mohammad, M. Dupuis, P. D. Funkenbusch, and D. H. Kelley, "Oscillating currents stabilize aluminium cells for efficient, low carbon production," arXiv preprint arXiv:2106.12606, 2021.